Heliyon 8 (2022) e10371

Contents lists available at ScienceDirect

Heliyon

journal homepage: www.cell.com/heliyon

Research article

Hyperactivation of mTOR and AKT in a cardiac hypertrophy animal model of Friedreich ataxia

Wing-Hang Tong [a], Hayden Ollivierre [a], Audrey Noguchi [b], Manik C. Ghosh [a], Danielle A. Springer [b], Tracey A. Rouault [a,*]

[a] Molecular Medicine Program, Eunice Kennedy Shriver National Institute of Child Health and Human Development, Bethesda, MD 20892, United States
[b] Murine Phenotyping Core, National Heart, Lung, and Blood Institute, Bethesda, MD 20892, United States

ARTICLE INFO

Keywords:
Friedreich ataxia
Cardiac hypertrophy
mTOR
AKT
Frataxin
FXN
ISCU
Iron-sulfur cluster biogenesis
Metabolic stress

ABSTRACT

Cardiomyopathy is a primary cause of death in Friedreich ataxia (FRDA) patients with defective iron-sulfur cluster (ISC) biogenesis due to loss of functional frataxin and in rare patients with functional loss of other ISC biogenesis factors. The mechanistic target of rapamycin (mTOR) and AKT signaling cascades that coordinate eukaryotic cell growth and metabolism with environmental inputs, including nutrients and growth factors, are crucial regulators of cardiovascular growth and homeostasis. We observed increased phosphorylation of AKT and dysregulation of multiple downstream effectors of mTORC1, including S6K1, S6, ULK1 and 4EBP1, in a cardiac/skeletal muscle specific FRDA conditional knockout (cKO) mouse model and in human cell lines depleted of ISC biogenesis factors. Knockdown of several mitochondrial metabolic proteins that are downstream targets of ISC biogenesis, including lipoyl synthase and subunit B of succinate dehydrogenase, also resulted in activation of mTOR and AKT signaling, suggesting that mTOR and AKT hyperactivations are part of the metabolic stress response to ISC deficiencies. Administration of rapamycin, a specific inhibitor of mTOR signaling, enhanced the survival of the Fxn cKO mice, providing proof of concept for the potential of mTOR inhibition to ameliorate cardiac disease in patients with defective ISC biogenesis. However, AKT phosphorylation remained high in rapamycin-treated Fxn cKO hearts, suggesting that parallel mTOR and AKT inhibition might be necessary to further improve the lifespan and healthspan of ISC deficient individuals.

1. Introduction

Iron-sulfur clusters (ISCs) constitute one of the most ubiquitous and functionally versatile classes of metallocofactor, serving essential functions in processes such as respiration, intermediary metabolism, and DNA repair. ISC biogenesis factors, such as frataxin (FXN) and the scaffold protein ISCU, are essential for synthesizing nascent ISCs that are transferred to target proteins or intermediate carriers with the assistance from many accessory proteins (Lill and Freibert, 2020; Maio and Rouault, 2020). Defects in ISC biogenesis are associated with dozens of human disorders, including the characteristic neurological and cardiac degeneration in FRDA and rare diseases such as the multiple mitochondrial dysfunctions syndromes (MMDS) caused by mutations in other ISC biogenesis factors (Tong, 2017). FRDA, the most prevalent inherited neuromuscular disorder, is caused by severely reduced transcription of frataxin (FXN) due to a large GAA repeat expansion within the first intron of the FXN gene (Campuzano et al., 1996; Puccio et al., 2001). More than 50% of FRDA patients develop hypertrophic cardiomyopathy that can progress to heart failure and death in the third to fifth decade of life (Hanson et al., 2019; Koeppen et al., 2015; Lane et al., 2013; Payne et al., 2011). Notably, cardiomyopathy has also been reported in several patients with mutations in other ISC biogenesis factors, including ISCU and BOLA3 (Haack et al., 2013; Kollberg et al., 2009).

Extensive studies have revealed that mTOR and AKT signaling cascades are part of a complex signaling network that mediates physiological and pathological cardiac hypertrophy (Heineke and Molkentin, 2006). mTOR complex I (mTORC1) plays a central role in regulating anabolic and catabolic processes, including protein synthesis, autophagy, metabolism and lysosomal function, in response to nutrient levels and growth factor signaling, while mTOR complex 2 (mTORC2) regulates the cytoskeleton, metabolism and several pro-survival pathways, including the AKT pathway (Saxton and Sabatini, 2017) (Figure 1A). In addition to sensing amino acid and glucose levels, mTORC1 is a downstream mediator of several growth factor and mitogen dependent signaling pathways,

* Corresponding author.
E-mail address: rouault@mail.nih.gov (T.A. Rouault).

https://doi.org/10.1016/j.heliyon.2022.e10371
Received 3 November 2021; Received in revised form 28 February 2022; Accepted 16 August 2022

including the insulin-like growth factor-I (IGF-I)–phosphatidylinositol 3-kinase (PI3K)–AKT pathway that triggers the Akt-dependent multisite phosphorylation and inhibition of TSC2 in the Tuberous Sclerosis Complex (TSC), which in turns inhibits mTORC1. Once activated, mTORC1 promotes protein synthesis by activating its substrates, p70 S6 kinase 1 (S6K1), which phosphorylates S6 ribosomal protein and eukaryotic initiation factor 4E (eIF4E)-binding protein 1 (4EBP1), and inhibits the early steps of autophagosome formation (via Unc-51 like kinase 1, ULK1) and lysosomal biogenesis (via transcription factor TFEB). In addition to activating mTORC1 signaling, hyperactivated AKT mediates the inhibitory phosphorylation of glycogen synthase kinase 3β (GSK3β). Active GSK3β negatively regulates cardiac hypertrophic transcriptional effectors, such as GATA4, β-catenin, c-Myc and nuclear factor of activated T cells (NFAT), but becomes inhibited by AKT-mediated phosphorylation (Heineke and Molkentin, 2006). Interestingly, both mTORC2-mediated phosphorylation of AKT at S473 and PI3K/PDK1-activated phosphorylation at T308 are needed for maximal AKT activity, which mechanistically place mTOR both upstream and downstream of AKT (Efeyan and Sabatini, 2010).

Aberrant activations of mTORC1 and AKT are well documented in many hypertrophic cardiomyopathies (Sciarretta et al., 2018). Mice with constitutive activation of Akt (Shioi et al., 2002) or cardiac deletions of Tsc genes (Malhowski et al., 2011; Taneike et al., 2016) exhibited hyperactivation of mTORC1, enlarged hearts, increased left ventricle (LV) wall thickness, and early death. Conversely, inhibition of mTORC1 attenuated hypertrophy in various cardiomyopathy models (Sciarretta et al., 2018). The links between mTOR/AKT hyperactivation and cardiomyopathies were further supported by the findings of cardiac hypertrophies in transgenic mice with overexpression of S6K1 (McMullen et al., 2004) and mice with cardiac deletions of Tsc genes (Malhowski et al., 2011; Taneike et al., 2016) or GSK3β ablation (Kerkela et al., 2008). In the present study, we report that mTOR and AKT pathways are hyperactivated in ISC biogenesis-deficient cells and tissues, and rapamycin treatment improves the survival of heart/skeletal muscle specific conditional Fxn knockout (cKO) mice.

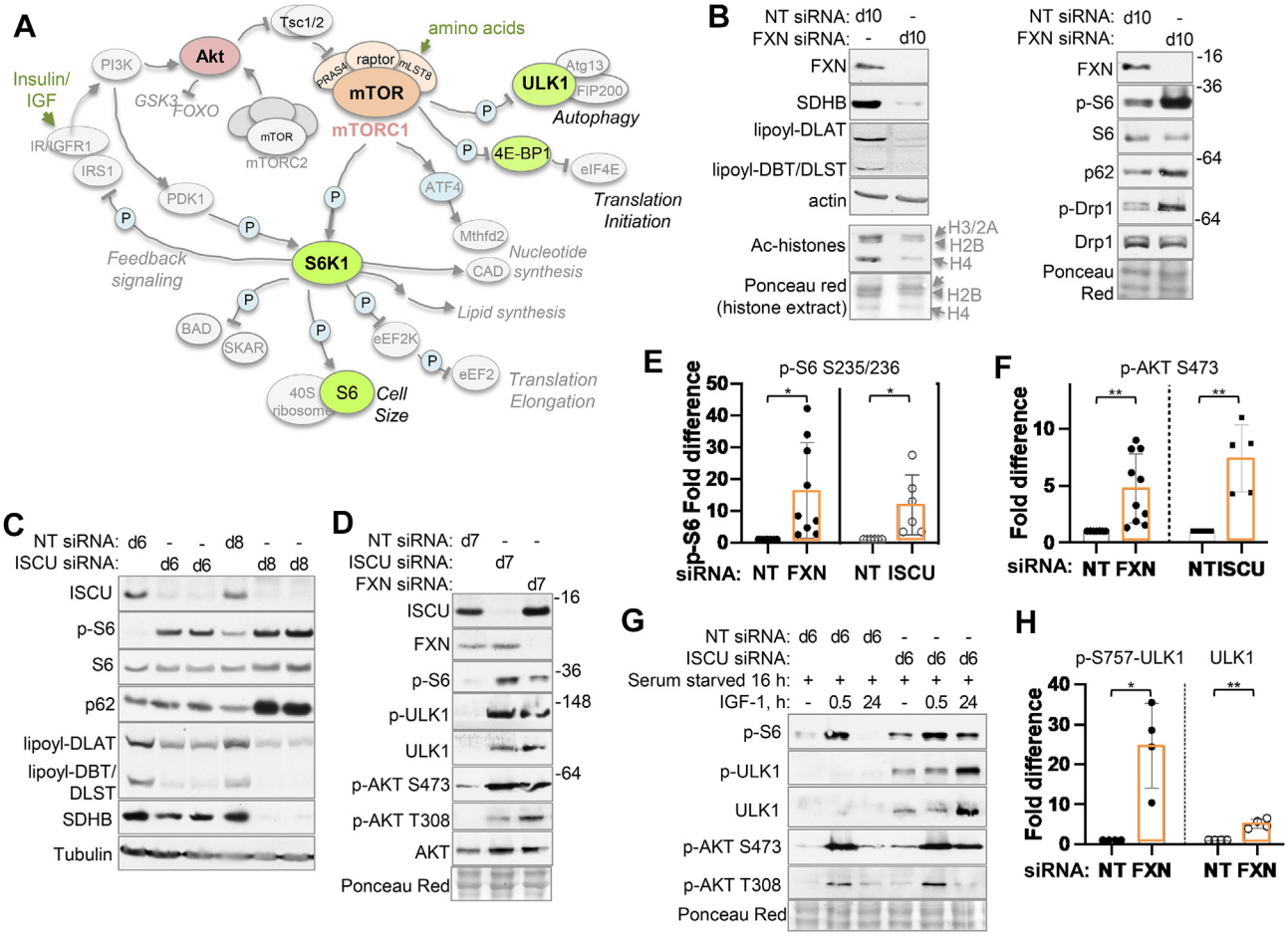

Figure 1. ISC deficiency induced activation of mTORC1 signaling cascade. (A) Schematic of mTOR and AKT signaling pathways in mediating physiological and pathological cardiac hypertrophy. mTORC1 signaling cascade balances mRNA translation, protein turnover and metabolism, in response to growth factors and nutrient levels, while mTORC2 regulates cytoskeleton, metabolism and activates several pro-survival pathways, including the AKT signaling pathway. In addition to sensing amino acid and glucose levels, mTORC1 is a downstream mediator of several growth factor pathways, including the insulin-like growth factor-I (IGF-I)–phosphatidylinositol 3-kinase (PI3K)–AKT pathway. In addition to activating mTORC1 signaling, hyperactivated AKT mediates the phosphorylation of other regulators of cardiac hypertrophy including GSK3β and folkhead transcription factors FOXO. (B) Knockdown (KD) of FXN not only resulted in a decreased in functional Fe–S proteins, as indicated by reduced lipoylation of DBT, DLST and DLAT by LIAS, decreased levels of respiratory complex II subunit SDHB, and decreased acetylation of histones (Tong et al., 2018), but also resulted in increased levels of p-S6, p62 and p-Drp1 in human fibroblasts MCH46 compared to cells transfected with non-targeting siRNA (NT siRNA). The full, uncropped versions are shown in the supplemental data (Figures S4 and 5). (C) KD of ISCU resulted in increased levels of p-S6 and p62. The uncropped versions are shown in Figure S6. (D) KD of FXN or ISCU resulted in increased levels of p-S6, p-S757-ULK1, ULK1, p-S473-AKT and p-T308-AKT. The uncropped versions are shown in Figure S7. (E) Densitometry analysis showed an increase in p-S6 levels in FXN or ISCU KD fibroblasts normalized to controls ($n > 6$). (F) Increased levels of p-AKT at S473 in FXN-KD ($n = 10$) and ISCU-KD ($n = 5$) cells normalized to NT-KD control cells. (G) KD of ISCU increased the levels of p-S6, p-S757-ULK1, ULK1, and p-S473-AKT in serum-starved human fibroblasts with or without IGF-1 stimulation compared to NT siRNA. The uncropped versions are shown in Figure S8. (H) Increased p-ULK1 and ULK1 levels in FXN-KD ($n = 4$) cells normalized to NT-KD control cells. The t-test significance P values are indicated (*$P < 0.05$; **$P < 0.005$). See also Figure S1.

2. Results

2.1. Hyperactivation of mTOR and AKT signaling in cells that are deficient in ISC biogenesis

ISC biogenesis factors have crucial roles in maintaining the functions and stability of many proteins that are important for cellular metabolism, including many subunits of the respiratory complexes (e.g. NDUFS1 and SDHB), cytosolic aconitase (ACO1, also known as iron regulatory protein 1 or IRP1), mitochondrial aconitases (ACO2), and lipoyl synthase (LIAS) which is essential for the lipoylation and activation of the DBT subunit of branched-chain ketoacid dehydrogenase (BCKDH), the DLAT subunit of pyruvate dehydrogenase (PDH), and the DLST subunit of alpha-ketoglutarate dehydrogenase (αKGDH). Interestingly, we have observed that chelation of iron not only resulted in the loss of functional Fe–S protein, as indicated by reduced levels of lipoyl-DBT, reduced ACO1 and ACO2 activities, and reduced stability of SDHB and NDUFS1 proteins, but also increased phosphorylation of S6K1 (at T389), S6 (at S235/236) and AKT (at S473) in human fibroblast MCH46 (Figure S1A-B). Because increased p-S6K1 and p-S6 levels are indicators of mTORC1 activation, and both elevated levels of branched-chain amino acids (BCAAs) (as a result of decreased BCKDH-mediated catabolism of leucine, isoleucine and valine) and activation of AKT have been shown to cause activation of mTORC1 signaling (Figure S1C) and organ hypertrophy (Neishabouri et al., 2015; Shioi et al., 2002), we tested whether interference with ISC biogenesis can cause mTORC1 and AKT activations. Indeed, small interfering RNA (siRNA)-knockdown (KD) of FXN and ISCU not only resulted in deceased LIAS activity and SDHB levels (Figure 1B, C), but also increased the levels of p-S6 and p-AKT (Figure 1B–F). Given that mTORC1 and AKT signalings are very sensitive to growth factor levels in the media, we also observed that KD of ISCU resulted in increased levels of p-S6 and p-S473-AKT in both serum-starved and IGF-1 stimulated human fibroblasts compared to non-targeting (NT) KD (Figure 1G).

In addition to promoting protein synthesis, mTORC1 regulates both general autophagy and mitophagy induction after oxidative phosphorylation uncoupling (Bartolome et al., 2017). mTORC1 is an important negative regulator of autophagy by phosphorylating S757 of ULK1, a kinase required for the initiation of autophagy (Kim et al., 2011). Previous studies have shown that, during prolonged stress, ULK1 transcription is upregulated, but the activity of newly synthesized ULK1 is inhibited by mTOR-mediated phosphorylation at S757 (Nazio et al., 2016). Dysregulated autophagy has been shown to increase the levels of the autophagy-adaptor protein p62/SQSTM1 (Huang et al., 2013; Mizushima et al., 2008), and an increase in p62 levels was observed with cardiac deletions of Tsc genes in mice (Edenharter et al., 2018; Kayyali et al., 2015; Taneike et al., 2016) and in a *Drosophila* model of FRDA (Edenharter et al., 2018; Kayyali et al., 2015; Taneike et al., 2016). In addition, increased mitochondrial fragmentation and dysregulation of dynamin-related protein 1 (DRP1), which plays an essential role in mediating mitochondrial fission and mitophagy (Tong et al., 2020), have been reported in various FRDA models (Johnson et al., 2021; Lin et al., 2017; Martelli et al., 2015). In FXN- or ISCU-KD cells, levels of ULK1 (Figure 1D, G, H), p-S757-ULK1 (Figure 1D, G, H), p62 (Figure 1B, C) and p-S616-DRP1 (Figure 1B) were all elevated, further suggesting that deficient ISC biogenesis leads to mTOR activation and dysregulation of autophagy and mitophagy.

2.2. Hyperactivation of mTORC1 in a cardiomyopathy model of Friedreich's ataxia

Next, we examined an animal model of FRDA cardiomyopathy. Fxn cKO (Fxn:Mck-Cre) mice have a >2 fold increase in heart/body weight ratio (Figure 2A) and a short median lifespan of 82 days (Figure 2B) compared to Fxn+/+ littermates, consistent with previous reports of a different cardiac/muscle specific Fxn cKO mouse (Puccio et al., 2001). Loss of Fxn not only resulted in loss of functional Fe–S proteins (Figure 2C) and dysregulation of iron-regulatory proteins 1 and 2 (Irp1 and Irp2) (Figure 2D), but also increased p-S6 levels in 5-week-old Fxn cKO hearts (Figure. 2E, G), and increased p-4ebp1, p-Akt, p-S757-Ulk1, p-Drp1, and p62 levels in 7- to 10-week-old Fxn cKO hearts (Figures 2F, G, S2A), consistent with mTORC1 and AKT hyperactivation. In contrast, Fxn cKO skeletal muscles did not show consistent hyperactivation of mTORC1 targets, despite extensive loss of Fxn and significant decrease in the levels of Ndufs1 and Sdhb proteins at 9 weeks (Figure S2B). These results are in line with the absence of significant skeletal muscle involvement in FRDA patients and other FRDA mouse models (Puccio et al., 2001).

2.3. Hyperactivation of mTORC1 and AKT signaling as a retrograde response to metabolic stress in cells with Fe–S enzyme deficiency

Since elevated levels of BCAAs as a result of decreased BCKDH activity are associated with cardiometabolic disorders (Sun et al., 2016) and exposure to BCAAs have been shown to cause activation of mTORC1 downstream targets (Saxton and Sabatini, 2017) (Figure 3A), we examined KD of the Fe–S protein LIAS that is essential for the lipoylation and activation of BCKDH (Figure 3B). LIAS KD not only decreased lipoylation of the DBT subunit of BCKDH, but also led to increased levels of p-S6K1, p-S6, p-S757-ULK1, ULK1, p-AKT, and p-Drp1 (Figure 3C–E). However, there was no difference in the lifespans of Fxn cKO mice that were fed isocaloric low protein (6%) or high protein (40%) diet (Figure 3F) or BCAA-enriched drinking water compared to control animals (Figure 3G). These results suggested that additional factors other than cardiac loss of functional BCKDH are involved in the early death of Fxn cKO mice.

Next, we examined mTOR and AKT signaling in KD of other proteins that require ISC for their functions (Figure 4A), and observed that KD of complex II subunit SDHB also increased the levels of p-S6K1, p-S6 and p-AKT (Figure 4B and C). Similarly, KD of dihydrolipoyl transacetylase (DLAT), a PDH subunit that does not contain ISC but is dependent on lipoylation by the Fe–S protein LIAS, also resulted in increases in the levels of p-S6K1, p-S6, p-S757-ULK1 and p-AKT (Figure 4D–E). Taken together, these data suggest that mTORC1 and AKT are activated in response to metabolic stress induced by defects in ISC biogenesis.

Since prolonged disruption of ISC biogenesis resulted in increased oxidative stress (Soriano et al., 2013) (Jauslin et al., 2002), and oxidative stress modulates AKT and mTORC1 signaling (Pelicano et al., 2006; Sarbassov and Sabatini, 2005), we also examined AKT and mTOR signaling in cells treated with a redox-cycling mitochondrial pro-oxidant menadione. While cells treated with a redox-cycling mitochondrial pro-oxidant menadione for 2 h have decreased levels of p-S6K1 and p-S6, longer treatment (24–72 h) led to decreased DBT lipoylation, decreased levels of SDHB and NDUFS1, and concurrent increase in the levels of p-S6K1, p-S6, and p-AKT (Figure 4F). These data suggested that oxidative stress induced by ISC deficiency may form a vicious cycle that leads to further disruption of mitochondrial function and exacerbation of maladaptive mTOR and AKT signaling.

2.4. Targeting mTOR pathway to alleviate FXN-driven cardiomyopathy

Inhibition of mTORC1 signaling by the FDA-approved drug rapamycin has been shown to attenuate cardiac hypertrophy in mouse models (Shioi et al., 2002) and kidney transplant recipients (Paoletti, 2018). Given that rapamycin has potentially serious side effects, including glucose intolerance, immunosuppression, hyperlipidemia, and decreased wound healing, different dosing paradigms of rapamycin have been tested to achieve efficacy with minimal drug toxicity (Arriola Apelo et al., 2016; Johnson et al., 2015). Daily rapamycin injection (8 mg/kg) for 4 days or a diet containing encapsulated rapamycin (eRAPA) for 3 weeks reduced p-S6 levels in Fxn cKO mice (Figure 5B-C), without increasing the levels of functional Fe–S proteins (Figure 5B–D). More importantly, the cohort of Fxn cKO mice that received rapamycin injection every other

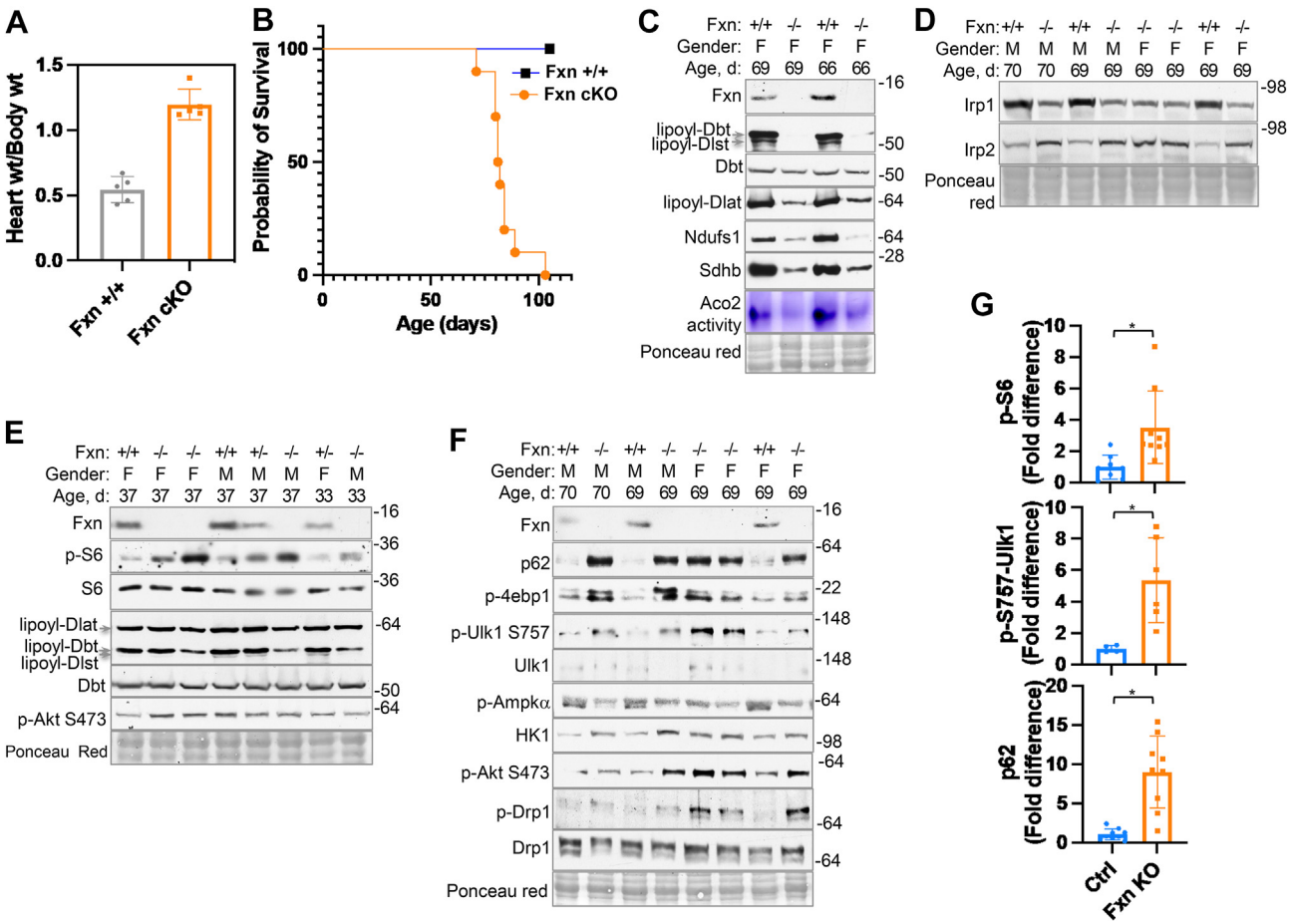

Figure 2. ISC deficiency induced activation of mTORC1 signaling cascade in a cardiac/skeletal muscle specific conditional knockout (Fxn cKO) mouse. (A) At 9–10 weeks of age, Fxn:Mck-Cre (Fxn cKO) mice (n = 5) had an increased heart weight/body weight ratio 1.18 +/− 0.12 compared to a wild-type ratio 0.54 +/− 0.1. (B) The median lifespan of Fxn cKO mice is 82 days (range 71–103 days), as compared to >24 months for wild-type mice. (C) Loss of functional Fe–S proteins (Ndufs1, Sdhb, Aco2, and LIAS) and dysregulation of mTORC1 downstream effects (S6K1, S6 and ULK1) in the hearts of Fxn cKO mice. The uncropped versions are shown in Figure S9. (D) Decreased levels of iron regulatory protein 1 (Irp1) and increased levels of Irp2 in the hearts of Fxn cKO mice. IRP1 and IRP2 are RNA-binding proteins that play important roles in the post-transcriptional regulation of intracellular iron metabolism, intermediary metabolism, and heme biosynthesis. The bifunctional IRP1 registers cytosolic iron levels rapidly through the assembly and disassembly of ISC in IRP1. Short term changes in ISC assembly in IRP1 results in a loss of its aconitase activity and an increase in binding to its mRNA targets, whereas prolonged loss of ISC in IRP1 results in decreased stability of the protein. In contrast, IRP2 is regulated by iron and oxygen-dependent protein degradation. Oxidation of an ISC in the F-box and leucine-rich repeats protein 5 (FBXL5), a substrate receptor subunit of an SKP1-CUL1-F box (SCF) ubiquitin ligase complex, promotes binding and degradation of IRP2 (Wang et al., 2020). The uncropped versions are shown in Figure S10. (E) At 5 weeks old, Fxn cKO mice have increased levels of p-S6 in the hearts. The uncropped versions are shown in Figure S11. (F) At 9 weeks or older, Fxn cKO hearts have increased levels of p62, p-S473-Akt, p-T37/46-4ebp1, p-S757-Ulk1 and p-Drp1. Phosphorylation of 4ebp1 by mTORC1 results in its dissociation from eIF4E, promoting assembly of the eIF4F complex. The uncropped versions are shown in Figure S12. (G) Increased levels of p-S6 (n = 9, 5–7 weeks of age), p-S757-Ulk1 (n = 6, 7–10 weeks of age) and p62 (n = 9, 7–10 weeks of age) in Fxn cKO hearts normalized to controls. The t-test significance P values are indicated (*P < 0.05; **P < 0.005). See also Figure S2.

day or eRAPA diet had increased median lifespans of 114 and 119 days, respectively, compared to 82 days for untreated and vehicle-treated Fxn cKO mice (Figures 5A, S3A). In comparison, the median lifespan of FXN cKO mice was only increased to 87 days (range 79–115 days) in the 4 days on-10 days off cohort (Figure S3B).

Although the lifespan of Fxn cKO mice that received rapamycin injection every other day or eRAPA diet increased by 40% (Figure 5A), these mice still died very early compared to $Fxn^{+/+}$ mice, primarily because of persistant deficiencies of functional Fe–S proteins. It is also interesting to note that, rapamycin treatment did not abrogate the increase in p-S473-Akt levels in many of the Fxn cKO mice (Figure 6A) nor resulted in statistical changes in the heart/body weight ratio (Figure S3C) and echocardiographic parameters (Figure S3D), suggesting that hyperactivation of Akt also contributes to cardiomyopathy in Fxn deficiency through mTORC1-independent mechanisms. Given the many metabolic and stress response pathways that can be affected by changes in mTOR signaling, the pleiotropic effects of rapamycin are of significant interest. Previous studies have shown that rapamycin induced the expression of tristetraprolin (Ttp), which decreased the expression of transferrin receptor 1 (TfR1) and ferroportin 1 (Fpn1) in wild type mouse embryonic fibroblasts (Bayeva et al., 2012). We observed that rapamycin treatment also resulted in a marked decrease in TfR1 levels in rapamycin-treated Fxn cKO hearts (Figure 6B). However, our data did not show a significant increase in Ttp levels or changes in Irp1, Irp2, and Fpn1 levels in rapamycin-treated compared to vehicle-treated Fxn cKO hearts (Figure 6B). Previous studies have also shown that rapamycin-treated mouse skin fibroblasts have increased levels of nuclear factor (erythroid-derived 2)-like2 (Nrf2), a major regulator of endogenous

antioxidant enzymes, such as NADPH: quinone oxidoreductase (NQO1), and Nrf2 activation has been shown to improve the cell viability and mitochondrial function in cells from FRDA patients (Rodden and Lynch, 2021). However, we did not observed an increase in Nqo1 protein level in our rapamycin-treated Fxn-cKO hearts (Figure 6B).

The finding of mTORC1 hyperactivation in Fxn cKO has important implications on several FRDA therapeutics under evaluation, including iron chelator deferiprone and IFN-γ therapies. As mentioned above, deferiprone treatment resulted in loss of functional Fe–S proteins as well as hyperphosphorylation of S6K1, S6 and AKT (Figure S1A), which can potentially exacerbate cardiac dysfunction in FRDA patients. Similarly, human fibroblasts treated with IFN-γ exhibited a rapid increase in p-AKT (Kaur et al., 2008), p-S6K1 and p-S6 levels (Figure 6C). Although transient, the mTOR/AKT activation in response to IFN-γ raises concern of additional cardiometabolic risk in patients administered these therapies. Taken together, our results suggest that the use of combination therapies consisting of mTORC1 and AKT inhibitors, antioxidants, and agents that boost the expression levels of FXN and other ISC biogenesis genes may be needed to further improve the healthspan and lifespan of patients with ISC biogenesis defects.

3. Discussion

Cardiac energy metabolism is essential for the normal biology and physiology of the heart, and metabolic flexibility is key for the heart to adapt to changes in fuel availability and stress (Ritterhoff and Tian, 2017). As a result, cardiomyopathy is observed in a plethora of metabolic disorders (Brown et al., 2017). Defects in ISC biogenesis in metabolic factors can lead to disruption of energy production, insufficient supply of anaplerotic intermediates, and NADH/NAD^+ imbalance, ultimately resulting in cardiomyopathy and heart failure. In addition to derailment of mitochondrial metabolism, cardiac cells with mitochondrial dysfunctions respond to the vicious cycles of redox imbalance, metabolic bottlenecks, altered protein acetylation, impaired Ca^{2+} homeostasis, and inflammation (Zhou and Tian, 2018) by activating signaling pathways to restore metabolic homeostasis (Heineke and Molkentin, 2006). The current study showed that ISC deficiency resulted in hyperactivation of both mTORC1 (as indicated by S6K1, S6, ULK1, and 4E-BP1 phosphorylation) and an increase in p-S473-AKT levels (a target of mTOCR2) *in vitro* and *in vivo*, consistent with a recent study showing increased mTOR signaling in a transgenic mouse model of inducible Fxn depletion (Vasquez-Trincado et al., 2021). AKT and mTOR signaling cascades are crucial for cardiovascular development, homeostasis, and stress response, but chronic AKT and mTOR activation has also been shown to lead to proteome imbalance, misfolded protein accumulation and energy stresses that promote the pathological remodeling of the heart (Sciarretta et al., 2018). In addition to driving protein synthesis through S6K1 and 4EBP1, mTORC1 can increase nucleotide synthesis via the ATF4-dependent expression of MTHFD2, a key component of the tetrahydrofolate cycle that provides one carbon units for purine synthesis

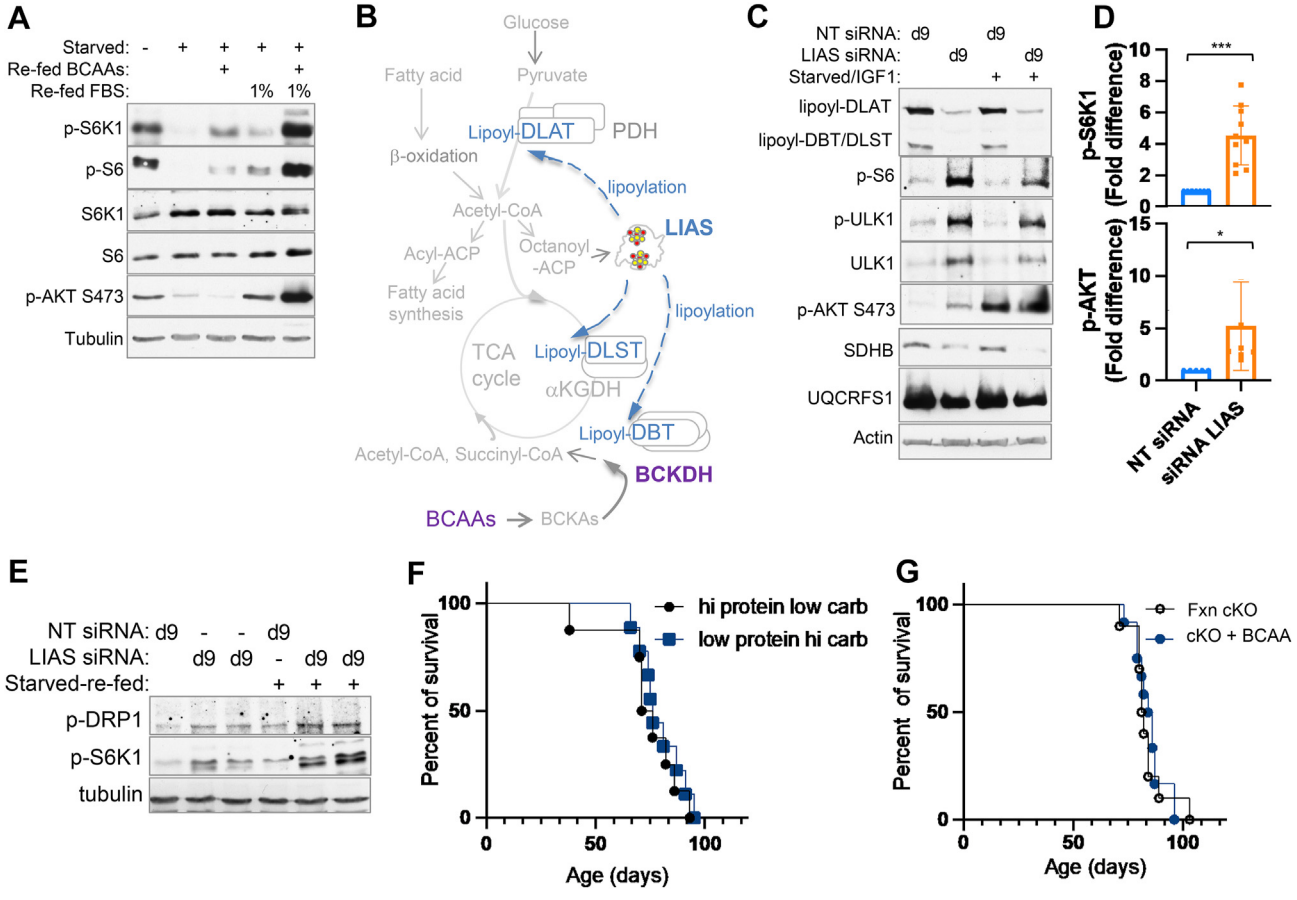

Figure 3. Defects in BCAA catabolism contributed to mTOR hyperactivation. (A) Withdrawal of BCAA and or fetal bovine serum (FBS) correlated with decreased phosphorylation of S6K1 and S6 levels, whereas addition of BCAAs and/or FBS for 20 min correlated with rapid restoration of p-S6K1 and p-S6 levels. The uncropped versions are shown in Figure S13. (B) Schematic showing that the Fe–S protein LIAS is essential for the lipoylation and activation of BCKDH, PDH, αKGDH and the glycine cleavage system. Disruption of BCKDH function resulted in BCAA accumulation that can activate mTORC1. (C) KD of LIAS not only decreased the levels of lipoyl-DBT, DLST and DLAT, but also increased the levels of p-S6, p-S757-ULK1, ULK1 and p-S473-AKT. The uncropped versions are shown in Figure S14. (D) Increased p-S6K1 and p-AKT levels in fibroblasts depleted of LIAS ($n > 8$). (E) Increased p-DRP1 levels in fibroblasts depleted of LIAS. The uncropped versions are shown in Figure S15. (F) No difference between survival of Fxn cKO mice that were fed a high protein-low carbohydrate ($n = 8$) or a low protein-high carbohydrate diet ($n = 10$). (G) No difference in the survival of Fxn cKO mice that were given control drinking water and BCAA-containing drinking water ($n = 12$).

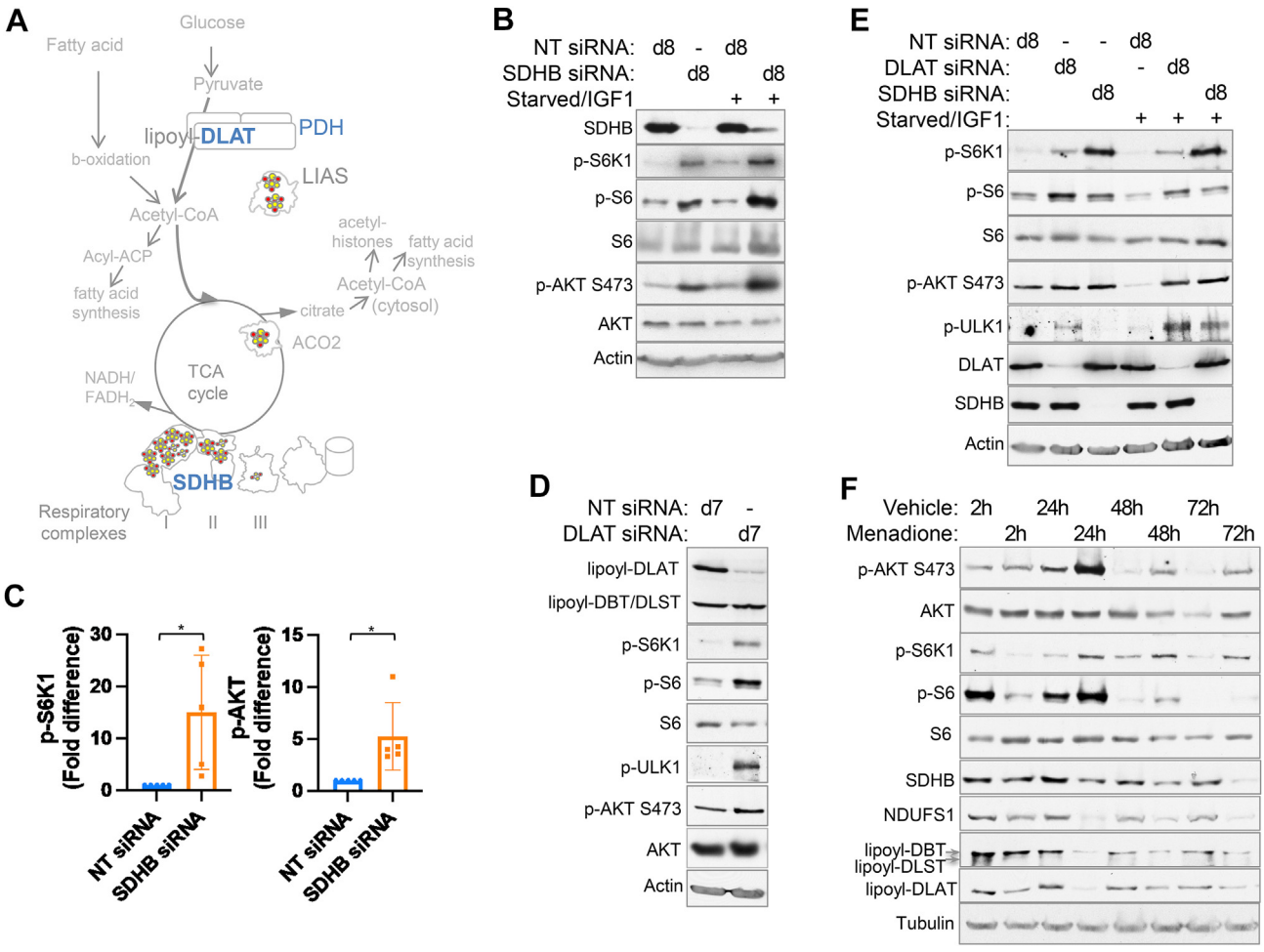

Figure 4. Hyperactivation of mTORC1 signaling in response to metabolic stress in cells with defects in Fe–S cluster biogenesis. (A) Schematic showing that ISC biogenesis controls the activities of proteins in many metabolic pathways, including SDHB, ACO2 and LIAS (which is essential for the lipoylation of BCKDH and PDH). (B) KD of the respiratory complex II subunit SDHB in human fibroblasts increased the levels of p-S6K1, p-S6, and p-S473-AKT in serum-replete cells and in cells that were starved of serum for 16 h and then restimulated with IGF-1 for 8 h. The uncropped versions are shown in Figure S16. (C) Increase in p-S6K1 and p-AKT levels in SDHB-KD cells (n = 5) normalized to NT-KD control cells (n = 5). (D) KD of PDH subunit DLAT increased levels of p-S6K1, p-S6, p-ULK1 and p-S473-AKT (n = 5). The uncropped versions are shown in Figure S17. (E) KD of DLAT or SDHB increased levels of p-S6K1, p-S6, p-ULK1 and p-S473-AKT in serum-repleted cells and in cells that were starved of serum for 16 h and then restimulated with IGF-1 for 24 h. The uncropped versions are shown in Figure S18. (F) Fibroblasts exposed to menadione for 24 h or longer exhibited decreased protein lipoylation, decreased SDHB and NDUFS1 levels, and increased levels of p-S6K1, p-S6, and p-S473-AKT (n = 5). The uncropped versions are shown in Figure S19.

(Ben-Sahra et al., 2016). Interestingly, Puccio and coworkers observed early elevation of Mthfd2 mRNA levels in their Fxn:Mck-Cre mice (Seznec et al., 2005), consistent with our results showing mTORC1 hyperactivation in the early stage of the cardiac disease in these animals. Activation of mTOR also inhibits autophagy and lysosome biogenesis (Saxton and Sabatini, 2017), which can lead to proteotoxic stress and compromised defense against oxidative stress to further potentiate cardiac dysfunction (Delbridge et al., 2017; Henning and Brundel, 2017). In addition to activating mTORC1 signaling, hyperactivated AKT mediates the inhibitory phosphorylation of GSK3β and FoxO transcription factors, which in turn regulate nuclear factor of activated T cells (NFAT) and other important mediators of cardiac health (Heineke and Molkentin, 2006).

The current study showed that multiple pathways downstream of decreased ISC biogenesis, including blockade of BCAA catabolism, metabolic and oxidative stress, and AKT activation, converge to activate the mTORC1 signalling cascade (Figure 6D). Congenital defects in BCAA catabolism, such as Maple syrup urine disease (MSUD), are associated with neurological dysfunction, cardiometabolic risks, and cardiac failure (Sun et al., 2016; Tobias et al., 2018), and are managed through low protein or low BCAA diet with some success (Blackburn et al., 2017). Although our experiments that were designed to manipulate BCAA level did not yield significant results (Figure 3F-G), it should be noted that, unlike FRDA patients (Stuwe et al., 2011), our Fxn cKO mice have normal hepatic Fxn levels. Previous studies have shown that a 15% restoration of BCKDH activity after hepatocyte transplantation into MSUD recipient liver was sufficient to restore normal blood BCAA levels and extended the lifespan in a MSUD mouse model (Skvorak et al., 2009). Furthermore, it should be noted that mTORC1 is also upregulated by other dietary factors including carbohydrate levels (Orozco et al., 2020). Thus, further studies of BCKDH activity and plasma BCAA levels in FRDA models and patients, and the potential risks and benefits of different diets that can affect mTORC1 signaling are needed.

To date, therapeutic options for ISC biogenesis disorders are limited (Tong, 2017; Zhang et al., 2019). Gene therapy restoring frataxin levels and nicotinamide mononucleotide therapy have improved the symptoms in FRDA mouse models but have not yet been translated to human therapies (Belbellaa et al., 2019; Martin et al., 2017). Our results demonstrated that inhibition of mTORC1 improves survival of Fxn cKO mice, which are consistent with previous studies that showed that genetic and pharmacological inhibition of TORC1 signaling produced improved motor performance and slightly increased lifespan of the FRDA KD flies

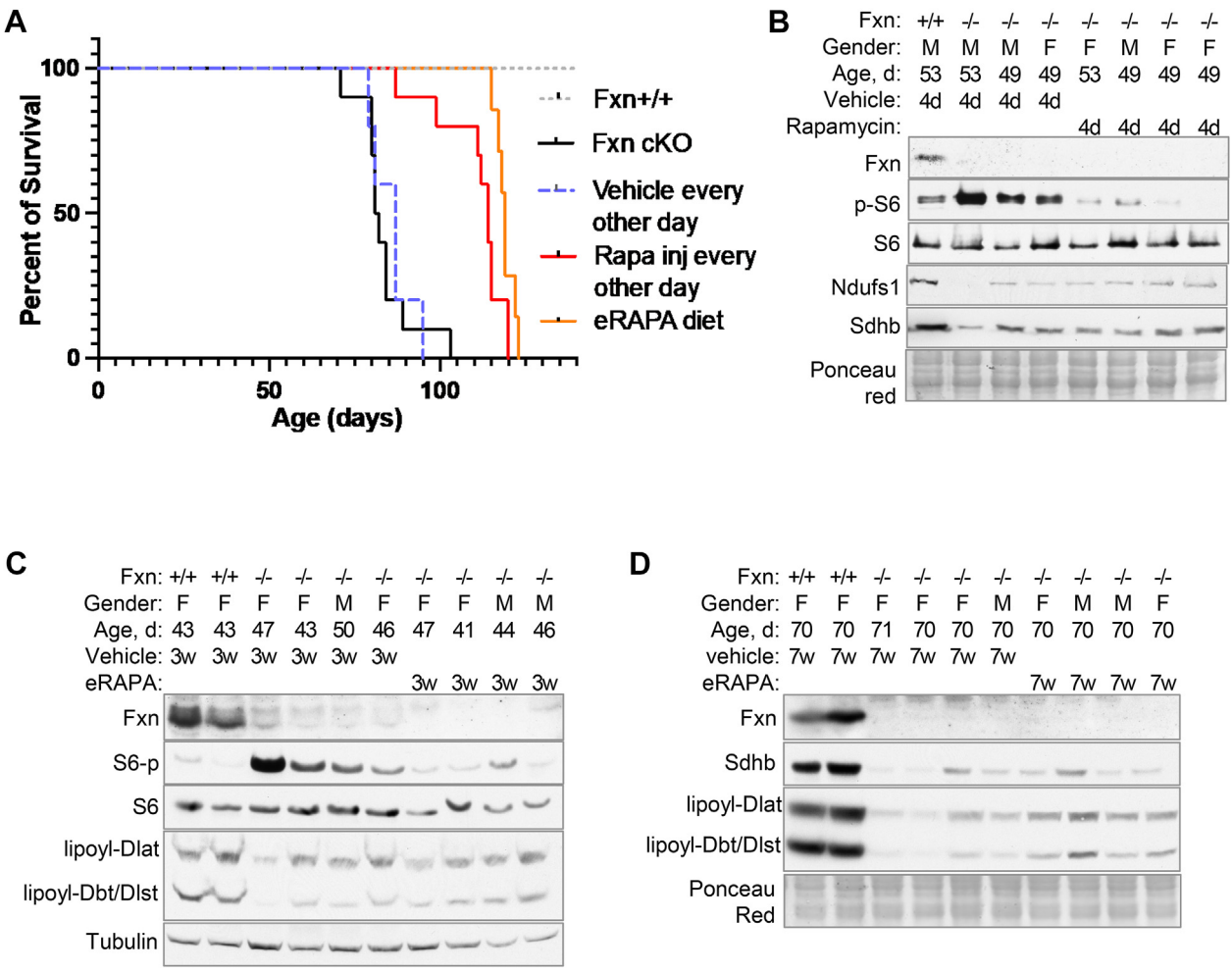

Figure 5. Inhibition of mTORC1 prolonged the survival of Fxn cKO mice. (A) Medium lifespan of Fxn cKO mice (n = 10) was extended from 81.5 days to 114 days (range = 87–120 days) by rapamycin injection every other day (n = 10) and to 119 days (range 115–123 days) by rapamycin-containing diet (n = 7). ($P < 0.0001$). There is no difference in lifespan between untreated and vehicle-treated cKO (n = 5). (B) Intraperitoneal injection of rapamycin for 4 consecutive days resulted in decreased levels of p-S6 in Fxn cKO mouse hearts, without changing the levels of Fxn, Ndufs1 and Sdhb. The uncropped versions are shown in Figure S20. (C) Dietary rapamycin treatment (42 ppm) for 3 weeks decreased p-S6 levels without increasing the levels of functional Fe–S proteins in Fxn cKO mouse hearts. The uncropped versions are shown in Figure S21. (D) Dietary rapamycin treatment (42 ppm) for 7 weeks did not increase the levels of functional Fe–S proteins. The uncropped versions are shown in Figure S22.

(Calap-Quintana et al., 2015), and improved survival and delayed neurological symptoms of the NDUFS4 KO mouse model of Leigh syndrome (Johnson et al., 2013). It is also interesting to note that p38 MAPK inhibitors reversed the growth defect of FRDA cells in culture (Cotticelli et al., 2018). Cancer studies have shown that mTORC1 functions as a downstream effector for the MAPK pathway, and a study in cardiac development showed that p38γ and p38δ promote cardiac hypertrophy by targeting the mTOR-inhibitory protein DEP domain-containing mTOR-interacting protein (DEPTOR) for degradation (Gonzalez-Teran et al., 2016).

In addition to mTORC1 hyperactivation, we also observed increased p-S473-AKT in FXN-KD, ISCU-KD, SDHB-KD, DLAT-KD and LIAS-KD fibroblasts, and in 7–9-week-old Fxn cKO hearts. Although short-term activation of Akt promotes physiological hypertrophy and protection from myocardial injury, long-term Akt activation causes cardiomyopathy via both mTOR-dependent and mTOR-independent mechanisms (Chaanine and Hajjar, 2011; Manning and Toker, 2017; Wende et al., 2015). Notably, rapamycin treatment did not mitigate the increase in p-S473-Akt levels in some Fxn cKO mice (Figure 6A). Extensive research has shown that a complex branching and looping positive and feedback signaling network modulates the function of mTOR and AKT (Efeyan and Sabatini, 2010; Manning and Toker, 2017). For instance, suppression of mTORC1 activity by rapamycin prevents the degradation of insulin receptor substrate 1 (IRS-1) and augments AKT activation in several cancer cell types, suggesting that the potential anti-hypertrophy activities of rapamycin can be counterbalanced by the release of feedback inhibition of AKT activation (Soares et al., 2013). A further understanding of mTORC1, mTORC2 and AKT signaling in ISC deficiency will be critical for clinical development for FRDA patients, since cancer studies suggested that parallel mTORC1 and PI3K/AKT inhibition might be necessary to control feedback loops (Sathe et al., 2018). Furthermore, the pleiotropic effects of rapamycin are of significant concern. Clinical studies have shown that chronic treatment with rapamycin are associated with the development of microcytic anemia (Przybylowski et al., 2013). We observed a marked decrease in TfR1 levels in Fxn cKO mice after 3–6 weeks of diet containing 42 ppm rapamycin, although no changes in other iron metabolism factors including Irp1, Irp2 and Fpn1 were observed (Figure 6B). Given the critical role of iron homeostasis in organismal health, great care must be given to determine treatment regimens to limit adverse effects on iron metabolism.

Taken together, our results pointed to aberrant mTORC1 and AKT signaling as mechanistic components of the cardiomyopathy associated with Fe–S protein deficiency and suggested that mTOR inhibitors may present much needed therapeutic opportunities for FRDA patients. The

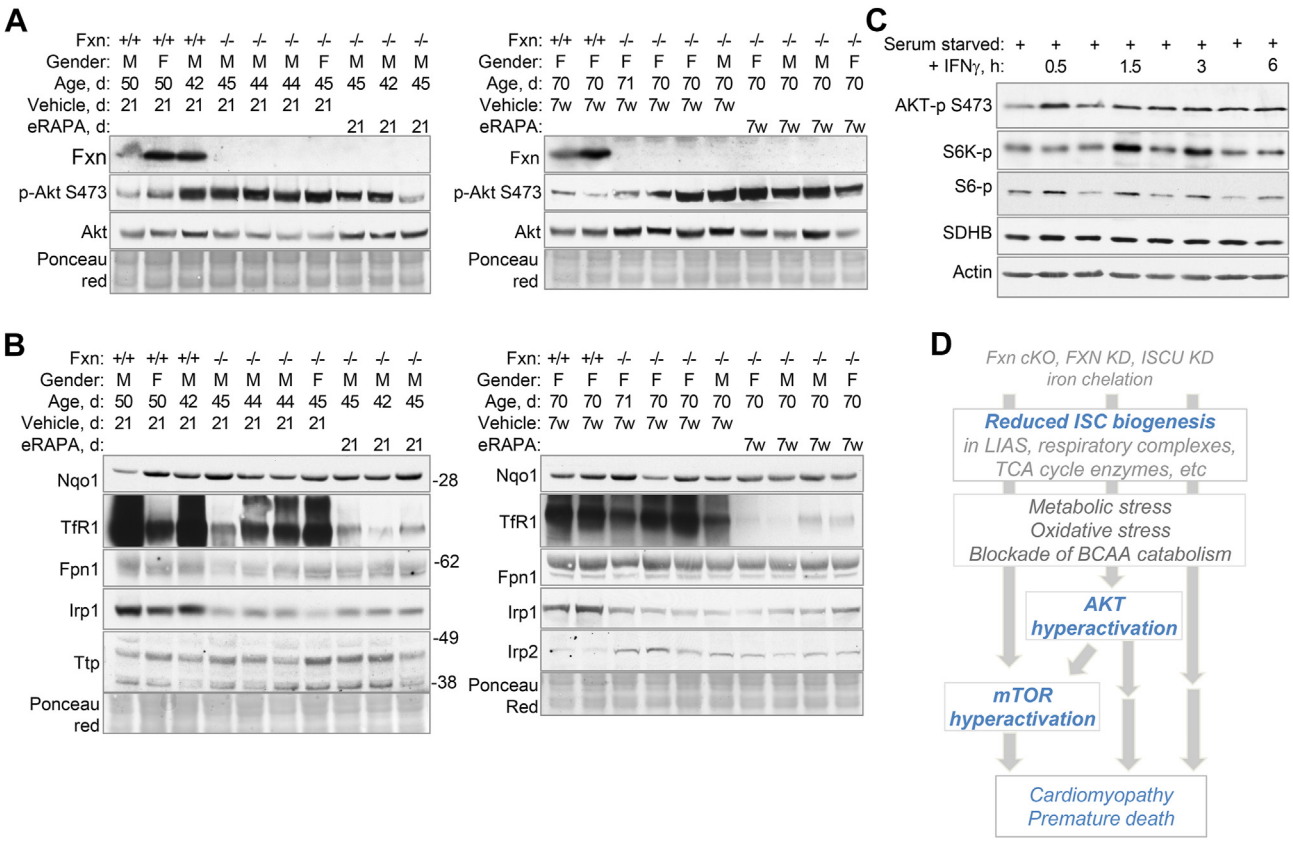

Figure 6. Persistent AKT hyperactivation and decreased TfR1 levels in rapamycin-treated Fxn cKO hearts. (A) Dietary rapamycin treatment did not abrogate Akt hyperphosphorylation in Fxn cKO hearts. The uncropped versions are shown in Figure S23. (B) Dietary rapamycin treatment resulted in decreased levels of the iron uptake protein transferrin receptor 1 (TfR1), but no significant changes in the levels of Nqo1, Irp1, Irp2, Fpn1 and Ttp in Fxn cKO hearts. The uncropped versions are shown in Figures S24 and 25. (C) Human fibroblasts treated with IFN-γ (5000U) resulted in a transient increase in the phosphorylation of Akt, followed by increased phosphorylation of S6K and S6, raising the concern of additional cardiometabolic risk in FRDA patients who are administered IFN- γ therapy. The uncropped versions are shown in Figure S26. (D) Schematic illustrating how metabolic stress, oxidative stress, and blockade of BCAA catabolism in response to ISC deficiency leads to hyperactivation of mTORC1 and Akt signaling which contributes to cardiomyopathy in Fxn cKO mice.

main concern in targeting the upstream and downstream factors of mTOR and AKT for therapeutic purposes is that each effector can have both adaptive and maladaptive influences on the myocardium and in the organismal level. Future studies should focus on evaluating the appropriate targets, intervention timing, dose-response profiles, and the use of combination therapies consisting of mTOR and AKT inhibitors, reduced BCAA diet, and direct augmentation of ISC biogenesis.

4. Resource availability

4.1. Lead Contact

Further information and requests for resources and reagents should be directed to and will be fulfilled by the Lead Contact, Tracey A Rouault (rouault@mail.nih.gov).

4.2. Materials availability

This study did not generate new unique reagents that have not been previously published in scientific literature.

5. Experimental model and subject details

5.1. Mouse models

Animal husbandry and veterinary care was provided by the NICHD Animal Facility. Experimental procedures were reviewed and approved by NICHD Animal Care and Use Committee and met NIH guidelines for the humane care of animals. Fxn^{flox} (homozygous frataxin floxed exon 2) mice with a CRISPR/Cas9-generated, Cre-conditional frataxin allele (#028520) and mice with heterozygous frataxin global KO and homozygous MCK-Cre (#029100) were obtained from the Jackson lab to generate the progressive cardiomyopathy mouse line $Fxn^{flox/null}$::MCK-Cre. *Fxn* heterozygous mice and wild-type mice are phenotypically indistinguishable and both are used as controls for the experiments described.

5.2. Cell cultures

HeLa cells were purchased from ATCC. Human dermal fibroblasts (MCH46) were a gift from Dr. Jessie Cameron (Hospital for Sick Children, Toronto, Canada). MCH46 and HeLa cells were cultivated in DMEM with 10% fetal bovine serum (FBS), 2 mM glutamine, and Antibiotic-Antimycotic (Invitrogen) at 37 °C in a humidified incubator containing 5% CO_2.

6. Method details

6.1. Mouse model experimental details

All mice were weaned at 20–21 days of age and fed Rodent NIH-07 Open Formula (410710-75-53) unless stated otherwise. Diet foods with 6%Protein /76% carbohydrate or 40% Protein/42% carbohydrate were purchased from Teklad custom diets. For BCAA supplementation, BCAAs

(300mM total) was dissolved in water with 0.02% culinary blue food color. For rapamycin intraperitoneal injections, rapamycin (LC laboratories) was dissolved in 100% ethanol to 100 mg/mL, then diluted in 5% PEG-400/5% Tween-20 (vehicle) to a concentration of 1.2 mg/mL, sterile filtered, aliquoted into 1 mL portions, and stored at −80 for long-term storage. Vehicle mice were injected with vehicle containing an equal volume of diluent lacking rapamycin. For dietary rapamycin experiments, encapsulated rapamycin (eRAPA) was obtained from Rapamycin Holdings, In., and mixed with eudragit (encapsulation material) into Purina LabDiet 5LG6 diet at PMI Nutrition International. Control food contained eudragit alone at a concentration matching that in the rapamycin chow.

6.2. Transfection and cell culture treatments

For KD experiments, cells were transfected every 3 days using On-TARGET Plus siRNA SMART Pools (30 nM) and Dharmafect 1 from Thermo Scientific. For growth factor starvation/refeeding experiments, the cells were placed in DMEM media with glutamine and without FBS for 8–16 h, and then stimulated with addition of 50 ng/mL insulin-like growth factor 1 (IGF-1) for 8–24 h, unless indicated otherwise. For amino acid starvation (Dyachok et al., 2016), the cells were placed in RPMI media with glutamine and without BCAAs and FBS for 100 min. Subsequently, the cells were stimulated with BCAA-replete RPMI with glutamine or L-amino acid solutions, with or without additional FBS, as indicated in the figure legends. Amino acids were diluted in H_2O, and the resulting solutions were filter sterilized and aliquots were kept at −20 °C.

6.3. Immunoblotting analysis

Whole-cell lysates were prepared using RIPA buffer containing 2 mM sodium citrate, Roche cOmplete Ultra protease inhibitor and PhosSTOP phosphatase inhibitor or Halt™ Protease Inhibitor Cocktail. Cut-up tissues were flash-frozen on dry ice. Tissues were homogenized with 5 volumes of RIPA buffer containing 2 mM sodium citrate, Roche cOmplete Ultra protease inhibitor and PhosSTOP phosphatase inhibitor or Halt™ Protease Inhibitor Cocktail at 4 °C using a bullet blender homogenizer Storm BBX24M. Blots were blocked in 5% milk-PBST and all primary antibodies were used 5% BSA-PBST or 5%-milk PBST following the manufacturer guidelines.

6.4. Activity assays

Mouse mitochondrial and cytosolic aconitase activities were assessed by in-gel aconitase assays as described previously (Tong and Rouault, 2006), with the following modifications. Non-denaturing gels composed of a separating gel containing 5% (for mouse lysates) or 7% (for human cell lysates), 133 mM Tris base, 66 mM borate, 3.6 mM citrate, and a stacking gel containing 5% acrylamide, 65 mM Tris base, 33 mM borate, 3.6 mM citrate. Whole-cell lysates were prepared using RIPA buffer containing 2 mM sodium citrate, Roche cOmplete Ultra protease inhibitor and/or PhosSTOP phosphatase inhibitor. Samples contain cell lysates, 25 mM Tris-Cl, pH 8.0, 10% glycerol, and 0.025% bromophenol blue. Electrophoresis was carried out at 180 V at 4 °C. Aconitase activities were assayed by incubating the gel in the dark at 37 °C in 100 mM Tris (pH 8.0), 1 mM NADP, 2.5 mM cis-aconitic acid, 5 mM MgCl2, 1.2 mM MTT, 0.3 mM phenazine methosulfate, and 5 U/ml isocitrate dehydrogenase, and quantitation was performed using NIH Image software.

6.5. Echocardiography

Transthoracic echocardiography was performed with 6–7 week old mice with a high-frequency ultrasound system (VisualSonics, Vevo 2100). All images were acquired using a MS-400 transducer (VisualSonics) with a center operating frequency of 30 MHz, and broadband frequency of 18–38 MHz. The axial resolution of this transducer is 50 mm, and the footprint is 20 mm 3 5 mm. 2D images were obtained for multiple views of the heart. Mmode images of the left ventricle were collected from the parasternal short axis view at the level of the mid-papillary muscles and obtained by rotating the probe 90″ clockwise from the parasternal long axis view. From the M mode images the LV systolic and diastolic posterior and anterior wall thicknesses, as well as end systolic and end diastolic internal LV chamber dimensions (LVIDs, LVIDd), were measured using the leading edge method.

7. Quantification and statistical analysis

Statistical analyses were performed by Student's *t* test for paired samples. Data are presented as means ± SEM. All data are representative of 3 or more independent experiments. The replicate and statistical details of experiments can be found in figure legends.

8. Key resources table

Reagent or resource	Source	Identifier
Antibodies		
FXN antibody	Proteintech	Cat#14147-1-AP; RRID:AB_2231876
ISCU antibody	(Tong and Rouault, 2006)	N/A
Phospho-p70 S6K (T389) antibody	Cell Signaling Technology	Cat#9205; RRID:AB_330944
Phosphor-S6 (S235/236) antibody	Cell Signaling Technology	Cat#2211; RRID:AB_331679
S6 antibody antibody	Cell Signaling Technology	Cat#2217; RRID:AB_331355
Phospho-AKT S473 antibody	Cell Signaling Technology	Cat#9271; RRID:AB_329825
Phospho-AKT T308 antibody	Cell Signaling Technology	Cat#2965; RRID:AB_2255933
AKT antibody	Cell Signaling Technology	Cat#9272; RRID:AB_329827
Phospho-ULK1 (S757) antibody	Cell Signaling Technology	Cat#14202; RRID:AB_266550
ULK1 antibody	Cell Signaling Technology	Cat#8054; RRID:AB_11178668
Phospho-4EBP1 (T37/46) antibody	Cell Signaling Technology	Cat#2855; RRID:AB_560835
SQSTM1/p62 antibody	Cell Signaling Technology	Cat#5114; RRID:AB_10624872
Phospho-AMPK (T172) antibody	Cell Signaling Technology	Cat#4188; RRID:AB_2169396 Cat# 2535; RRID:AB_331250
Hexokinase I (HK1) antibody	Cell Signaling Technology	Cat#2024; RRID:AB_2116996
DBT antibody	Proteintech	Cat#12451-1-AP; RRID:AB_2089636
Lipoic acid antibody	Millipore/ Calbiochem	Cat#437695; RRID:AB_10683357
Rabbit monoclonal anti-NDUFS1	Abcam	Cat#ab169540; RRID:AB_2687932
Mouse monoclonal anti-SDHA	Abcam	Cat#ab14715; RRID:AB_301433
Mouse monoclonal anti-SDHB	Abcam	Cat#ab14714; RRID:AB_301432
DRP1 antibody	Cell Signaling Technology	**Cat#5391;** RRID:AB_11178938
Phospho-DRP1 (S616) antibody	Cell Signaling Technology	Cat#4494; RRID:AB_11178659
Rabbit monoclonal anti-UQCRFS1	Abcam	Cat#ab191078; RRID:AB_2687933
Rabbit polyclonal anti-ACO2	T.A. Rouault	Epitope: YDLLEKNINI VRKRLNR

(*continued on next page*)

(*continued*)

Reagent or resource	Source	Identifier
Chemicals, peptides, and recombinant proteins		
Dulbecco's Modification of Eagle's medium (DMEM)	Cellgro	Cat#15013
RPMI 1640 Medium w/L-glutamine	USBiological	Cat#R8999
RPMI 1640 Medium w/L-glutamine, w/o BCAA	USBiological	Cat#R8990-20
L-leucine	Alfa Aesar	Cat#J62824
NADP	Sigma	Cat#N-0505
Cis-aconitate	Sigma	Cat#A3412
MTT	Sigma	Cat#M2128
Phenazine Methosulfate	Sigma	Cat#P-9625
isocitrate dehydrogenase	Sigma	Cat#I-2002
ProtoGel (30%)	National Diagnostic	Cat#EC-890
Deferiprone	Sigma	Cat#379409
Human recombinant insulin-like growth factor IGF-1	Peprotech	100–11
Menadione sodium bisulfite	Sigma	M2518
Rapamycin	LC laboratories	Rapamycin
Encapsulated rapamycin	rapamycin holding	Encapsulated rapamycin
Rodent NIH-07 Open Formula	VWR	Cat#410710-75-53
6% Protein Diet	Envigo Teklad Diets	Cat#TD.90016
40% Protein Diet	Envigo Teklad Diets	Cat#/TD.90018
Purina LabDiet 5LG6 diet containing encapsulated rapamycin	PMI Nutrition International	5LG6 with eRAPA
Purina LabDiet 5LG6 diet containing eudragit (capsule material)	PMI Nutrition International	5LG6 with eudragit
Human IFN-g	Peprotech	300–02
Krebs-Ringer Solution, bicarbonate-buffered	Alfa Aesar	Cat#J67591
NativePAGE 4–16% Bis-Tris Protein Gels, 1.0 mm	Thermo Fisher Scientific	Cat#BN1004BOX
Dharmafect1 Transfection Reagent	Dharmacon	Cat#T-2001-03
SuperSignal West Femto Maximum Sensitivity Substrate	Thermo Scientific	Cat#34096
Halt™ Protease Inhibitor Cocktail, EDTA-free (100X)	Thermo Scientific	Cat#78425
Pierce RIPA buffer	Thermo Scientific	cat#89900
Experimental models: Cell lines		
HeLa	ATCC	Cat#CCL-2; RRID:CVCL_0030

(*continued on next page*)

(*continued*)

Reagent or resource	Source	Identifier
MCH46 human fibroblast	a gift from Hospital for Sick Children, Toronto, Canada	
Experimental models: Organisms/strains		
C57BL/6J-congenic Fxn	Jackson Laboratory	Cat#028520
C57BL/6-congenic Fxn Tg (Ckmm-cre) 5Khn	Jackson Laboratory	Cat#029100
Oligonucleotides		
ON-TARGETplus Non-targeting Pool	Dharmacon	Cat#D-001810-10-05
ON-TARGETplus human FXN	Dharmacon	Cat#L-006691-00-0005
ON-TARGETplus human ISCU	Dharmacon	Cat#L-012837-01-0005
ON-TARGETplus human LIAS		Cat#L-010023-01-0005
ON-TARGETplus human SDH	Dharmacon	Cat#L-011773-02-0005
ON-TARGETplus human DLAT	Dharmacon	Cat#L-008490-01-0005
Software and algorithms		
GraphPad Prism 5	GraphPad Software	https://www.graphpad.com/scientificsoftware/prism/#1

Declarations

Author contribution statement

Wing-Hang Tong: Conceived and designed the experiments; Performed the experiments; Analyzed and interpreted the data; Wrote the paper.

Hayden Ollivierre: Performed the experiments.

Audrey Noguchi; Danielle A. Springer: Performed the experiments; Analyzed and interpreted the data.

Manik Ghosh: Contributed reagents, materials, analysis tools or data.

Tracey Rouault: Contributed reagents, materials, analysis tools or data; Wrote the paper.

Funding statement

Tracey A Rouault was supported by Eunice Kennedy Shriver National Institute of Child Health and Human Development [ZIAHD008814].

Data availability statement

Data included in article/supp. material/referenced in article.

Declaration of interest's statement

The authors declare no conflict of interest.

Additional information

Supplementary content related to this article has been published online at https://doi.org/10.1016/j.heliyon.2022.e10371.

Acknowledgements

The authors thank their colleagues at NIH and Dr Suh Young Jeong at Oregon Health and Science University for constructive discussions.

References

Arriola Apelo, S.I., Pumper, C.P., Baar, E.L., Cummings, N.E., Lamming, D.W., 2016. Intermittent administration of rapamycin extends the life span of female C57BL/6J Mice. J. Gerontol. Ser. A, Biol. Sci. Med. Sci. 71, 876–881.

Bartolome, A., Garcia-Aguilar, A., Asahara, S.I., Kido, Y., Guillen, C., Pajvani, U.B., Benito, M., 2017. MTORC1 regulates both general autophagy and mitophagy induction after oxidative phosphorylation uncoupling. Molecular and cellular biology 37.

Bayeva, M., Khechaduri, A., Puig, S., Chang, H.C., Patial, S., Blackshear, P.J., Ardehali, H., 2012. mTOR regulates cellular iron homeostasis through tristetraprolin. Cell Metabol. 16, 645–657.

Belbellaa, B., Reutenauer, L., Monassier, L., Puccio, H., 2019. Correction of half the cardiomyocytes fully rescue Friedreich ataxia mitochondrial cardiomyopathy through cell-autonomous mechanisms. Hum. Mol. Genet. 28, 1274–1285.

Ben-Sahra, I., Hoxhaj, G., Ricoult, S.J.H., Asara, J.M., Manning, B.D., 2016. mTORC1 induces purine synthesis through control of the mitochondrial tetrahydrofolate cycle. Science 351, 728–733.

Blackburn, P.R., Gass, J.M., Vairo, F.P.E., Farnham, K.M., Atwal, H.K., Macklin, S., Klee, E.W., Atwal, P.S., 2017. Maple syrup urine disease: mechanisms and management. Appl. Clin. Genet. 10, 57–66.

Brown, D.A., Perry, J.B., Allen, M.E., Sabbah, H.N., Stauffer, B.L., Shaikh, S.R., Cleland, J.G., Colucci, W.S., Butler, J., Voors, A.A., et al., 2017. Expert consensus document: Mitochondrial function as a therapeutic target in heart failure. Nat. Rev. Cardiol. 14, 238–250.

Calap-Quintana, P., Soriano, S., Llorens, J.V., Al-Ramahi, I., Botas, J., Molto, M.D., Martinez-Sebastian, M.J., 2015. TORC1 Inhibition by Rapamycin Promotes Antioxidant Defences in a Drosophila Model of Friedreich's Ataxia. PloS one 10, e0132376.

Campuzano, V., Montermini, L., Molto, M.D., Pianese, L., Cossee, M., Cavalcanti, F., Monros, E., Rodius, F., Duclos, F., Monticelli, A., et al., 1996. Friedreich's ataxia: autosomal recessive disease caused by an intronic GAA triplet repeat expansion. Science 271, 1423–1427.

Chaanine, A.H., Hajjar, R.J., 2011. AKT signalling in the failing heart. Eur. J. Heart Fail. 13, 825–829.

Cotticelli, M.G., Xia, S., Kaur, A., Lin, D., Wang, Y., Ruff, E., Tobias, J.W., Wilson, R.B., 2018. Identification of p38 MAPK as a novel therapeutic target for Friedreich's ataxia. Sci. Rep. 8, 5007.

Delbridge, L.M.D., Mellor, K.M., Taylor, D.J., Gottlieb, R.A., 2017. Myocardial stress and autophagy: mechanisms and potential therapies. Nat. Rev. Cardiol. 14, 412–425.

Dyachok, J., Earnest, S., Iturraran, E.N., Cobb, M.H., Ross, E.M., 2016. Amino Acids Regulate mTORC1 by an Obligate Two-step Mechanism. J. Biol. Chem. 291, 22414–22426.

Edenharter, O., Schneuwly, S., Navarro, J.A., 2018. Mitofusin-Dependent ER Stress Triggers Glial Dysfunction and Nervous System Degeneration in a Drosophila Model of Friedreich's Ataxia. Front. Mol. Neurosci. 11, 38.

Efeyan, A., Sabatini, D.M., 2010. mTOR and cancer: many loops in one pathway. Curr. Opin. Cell Biol. 22, 169–176.

Gonzalez-Teran, B., Matesanz, N., Nikolic, I., Verdugo, M.A., Sreeramkumar, V., Hernandez-Cosido, L., Mora, A., Crainiciuc, G., Saiz, M.L., Bernardo, E., et al., 2016. p38gamma and p38delta reprogram liver metabolism by modulating neutrophil infiltration. EMBO J. 35, 536–552.

Haack, T.B., Rolinski, B., Haberberger, B., Zimmermann, F., Schum, J., Strecker, V., Graf, E., Athing, U., Hoppen, T., Wittig, I., et al., 2013. Homozygous missense mutation in BOLA3 causes multiple mitochondrial dysfunctions syndrome in two siblings. J. Inherited Metabol. Dis. 36, 55–62.

Hanson, E., Sheldon, M., Pacheco, B., Alkubeysi, M., Raizada, V., 2019. Heart disease in Friedreich's ataxia. World J. Cardiol. 11, 1–12.

Heineke, J., Molkentin, J.D., 2006. Regulation of cardiac hypertrophy by intracellular signalling pathways. Nat. Rev. Mol. Cell Biol. 7, 589–600.

Henning, R.H., Brundel, B., 2017. Proteostasis in cardiac health and disease. Nat. Rev. Cardiol. 14, 637–653.

Huang, M.L., Sivagurunathan, S., Ting, S., Jansson, P.J., Austin, C.J., Kelly, M., Semsarian, C., Zhang, D., Richardson, D.R., 2013. Molecular and functional alterations in a mouse cardiac model of Friedreich ataxia: activation of the integrated stress response, eIF2alpha phosphorylation, and the induction of downstream targets. Am. J. Pathol. 183, 745–757.

Jauslin, M.L., Wirth, T., Meier, T., Schoumacher, F., 2002. A cellular model for Friedreich Ataxia reveals small-molecule glutathione peroxidase mimetics as novel treatment strategy. Hum. Mol. Genet. 11, 3055–3063.

Johnson, J., Mercado-Ayon, E., Clark, E., Lynch, D., Lin, H., 2021. Drp1-dependent peptide reverse mitochondrial fragmentation, a homeostatic response in Friedreich ataxia. Pharmacol. Res. Perspect. 9, e00755.

Johnson, S.C., Yanos, M.E., Bitto, A., Castanza, A., Gagnidze, A., Gonzalez, B., Gupta, K., Hui, J., Jarvie, C., Johnson, B.M., et al., 2015. Dose-dependent effects of mTOR inhibition on weight and mitochondrial disease in mice. Front. Genet. 6, 247.

Johnson, S.C., Yanos, M.E., Kayser, E.B., Quintana, A., Sangesland, M., Castanza, A., Uhde, L., Hui, J., Wall, V.Z., Gagnidze, A., et al., 2013. mTOR inhibition alleviates mitochondrial disease in a mouse model of Leigh syndrome. Science 342, 1524–1528.

Kaur, S., Sassano, A., Dolniak, B., Joshi, S., Majchrzak-Kita, B., Baker, D.P., Hay, N., Fish, E.N., Platanias, L.C., 2008. Role of the Akt pathway in mRNA translation of interferon-stimulated genes. Proc. Natl. Acad. Sci. U. S. A. 105, 4808–4813.

Kayyali, U.S., Larsen, C.G., Bashiruddin, S., Lewandowski, S.L., Trivedi, C.M., Warburton, R.R., Parkhitko, A.A., Morrison, T.A., Henske, E.P., Chekaluk, Y., et al., 2015. Targeted deletion of Tsc1 causes fatal cardiomyocyte hyperplasia independently of afterload. Cardiovasc. Pathol.: Off. J. Soc. Cardiovasc. Pathol. 24, 80–93.

Kerkela, R., Kockeritz, L., Macaulay, K., Zhou, J., Doble, B.W., Beahm, C., Greytak, S., Woulfe, K., Trivedi, C.M., Woodgett, J.R., et al., 2008. Deletion of GSK-3beta in mice leads to hypertrophic cardiomyopathy secondary to cardiomyoblast hyperproliferation. J. Clin. Invest. 118, 3609–3618.

Kim, J., Kundu, M., Viollet, B., Guan, K.L., 2011. AMPK and mTOR regulate autophagy through direct phosphorylation of Ulk1. Nat Cell Biol. 13, 132–141.

Koeppen, A.H., Ramirez, R.L., Becker, A.B., Bjork, S.T., Levi, S., Santambrogio, P., Parsons, P.J., Kruger, P.C., Yang, K.X., Feustel, P.J., et al., 2015. The pathogenesis of cardiomyopathy in Friedreich ataxia. PloS One 10, e0116396.

Kollberg, G., Tulinius, M., Melberg, A., Darin, N., Andersen, O., Holmgren, D., Oldfors, A., Holme, E., 2009. Clinical manifestation and a new ISCU mutation in iron-sulphur cluster deficiency myopathy. Brain 132, 2170–2179.

Lane, D.J., Huang, M.L., Ting, S., Sivagurunathan, S., Richardson, D.R., 2013. Biochemistry of cardiomyopathy in the mitochondrial disease Friedreich's ataxia. Biochem. J. 453, 321–336.

Lill, R., Freibert, S.A., 2020. Mechanisms of mitochondrial iron-sulfur protein biogenesis. Ann. Rev. Biochem.

Lin, H., Magrane, J., Rattelle, A., Stepanova, A., Galkin, A., Clark, E.M., Dong, Y.N., Halawani, S.M., Lynch, D.R., 2017. Early cerebellar deficits in mitochondrial biogenesis and respiratory chain complexes in the KIKO mouse model of Friedreich ataxia. Dis. Model Mech. 10, 1343–1352.

Maio, N., Rouault, T.A., 2020. Outlining the complex pathway of mammalian Fe-S cluster biogenesis. Trends Biochem. Sci. 45, 411–426.

Malhowski, A.J., Hira, H., Bashiruddin, S., Warburton, R., Goto, J., Robert, B., Kwiatkowski, D.J., Finlay, G.A., 2011. Smooth muscle protein-22-mediated deletion of Tsc1 results in cardiac hypertrophy that is mTORC1-mediated and reversed by rapamycin. Hum. Mol. Genet. 20, 1290–1305.

Manning, B.D., Toker, A., 2017. AKT/PKB signaling: navigating the network. Cell 169, 381–405.

Martelli, A., Schmucker, S., Reutenauer, L., Mathieu, J.R.R., Peyssonnaux, C., Karim, Z., Puy, H., Galy, B., Hentze, M.W., Puccio, H., 2015. Iron regulatory protein 1 sustains mitochondrial iron loading and function in frataxin deficiency. Cell Metabol. 21, 311–323.

Martin, A.S., Abraham, D.M., Hershberger, K.A., Bhatt, D.P., Mao, L., Cui, H., Liu, J., Liu, X., Muehlbauer, M.J., Grimsrud, P.A., et al., 2017. Nicotinamide mononucleotide requires SIRT3 to improve cardiac function and bioenergetics in a Friedreich's ataxia cardiomyopathy model. JCI Insight 2.

McMullen, J.R., Sherwood, M.C., Tarnavski, O., Zhang, L., Dorfman, A.L., Shioi, T., Izumo, S., 2004. Inhibition of mTOR signaling with rapamycin regresses established cardiac hypertrophy induced by pressure overload. Circulation 109, 3050–3055.

Mizushima, N., Levine, B., Cuervo, A.M., Klionsky, D.J., 2008. Autophagy fights disease through cellular self-digestion. Nature 451, 1069–1075.

Nazio, F., Carinci, M., Valacca, C., Bielli, P., Strappazzon, F., Antonioli, M., Ciccosanti, F., Rodolfo, C., Campello, S., Fimia, G.M., et al., 2016. Fine-tuning of ULK1 mRNA and protein levels is required for autophagy oscillation. J. Cell Biol. 215, 841–856.

Neishabouri, S.H., Hutson, S.M., Davoodi, J., 2015. Chronic activation of mTOR complex 1 by branched chain amino acids and organ hypertrophy. Amino Acids 47, 1167–1182.

Orozco, J.M., Krawczyk, P.A., Scaria, S.M., Cangelosi, A.L., Chan, S.H., Kunchok, T., Lewis, C.A., Sabatini, D.M., 2020. Dihydroxyacetone phosphate signals glucose availability to mTORC1. Nat. Metab. 2, 893–901.

Paoletti, E., 2018. mTOR inhibition and cardiovascular diseases: cardiac hypertrophy. Transplantation 102, S41–S43.

Payne, R.M., Pride, P.M., Babbey, C.M., 2011. Cardiomyopathy of Friedreich's ataxia: use of mouse models to understand human disease and guide therapeutic development. Pediatr. Cardiol. 32, 366–378.

Pelicano, H., Xu, R.H., Du, M., Feng, L., Sasaki, R., Carew, J.S., Hu, Y., Ramdas, L., Hu, L., Keating, M.J., et al., 2006. Mitochondrial respiration defects in cancer cells cause activation of Akt survival pathway through a redox-mediated mechanism. J. Cell Biol. 175, 913–923.

Przybylowski, P., Malyszko, J.S., Macdougall, I.C., Malyszko, J., 2013. Iron metabolism, hepcidin, and anemia in orthotopic heart transplantation recipients treated with mammalian target of rapamycin. Transpl. Proc. 45, 387–390.

Puccio, H., Simon, D., Cossee, M., Criqui-Filipe, P., Tiziano, F., Melki, J., Hindelang, C., Matyas, R., Rustin, P., Koenig, M., 2001. Mouse models for Friedreich ataxia exhibit cardiomyopathy, sensory nerve defect and Fe-S enzyme deficiency followed by intramitochondrial iron deposits. Nat. Genet. 27, 181–186.

Rensing, N., Han, L., Wong, M., 2015. Intermittent dosing of rapamycin maintains antiepileptogenic effects in a mouse model of tuberous sclerosis complex. Epilepsia 56, 1088–1097.

Ritterhoff, J., Tian, R., 2017. Metabolism in cardiomyopathy: every substrate matters. Cardiovasc. Res. 113, 411–421.

Rodden, L.N., Lynch, D.R., 2021. Designing phase II clinical trials in Friedreich ataxia. Expert Opin. Emerg. Drugs 26, 415–423.

Sarbassov, D.D., Sabatini, D.M., 2005. Redox regulation of the nutrient-sensitive raptor-mTOR pathway and complex. J. Biol. Chem. 280, 39505–39509.

Sathe, A., Chalaud, G., Oppolzer, I., Wong, K.Y., von Busch, M., Schmid, S.C., Tong, Z., Retz, M., Gschwend, J.E., Schulz, W.A., et al., 2018. Parallel PI3K, AKT and mTOR inhibition is required to control feedback loops that limit tumor therapy. PloS One 13, e0190854.

Saxton, R.A., Sabatini, D.M., 2017. mTOR signaling in growth, metabolism, and disease. Cell 168, 960–976.

Sciarretta, S., Forte, M., Frati, G., Sadoshima, J., 2018. New insights into the role of mTOR signaling in the cardiovascular system. Circul. Res. 122, 489–505.

Seznec, H., Simon, D., Bouton, C., Reutenauer, L., Hertzog, A., Golik, P., Procaccio, V., Patel, M., Drapier, J.C., Koenig, M., et al., 2005. Friedreich ataxia: the oxidative stress paradox. Hum. Mol. Genet. 14, 463–474.

Shioi, T., McMullen, J.R., Kang, P.M., Douglas, P.S., Obata, T., Franke, T.F., Cantley, L.C., Izumo, S., 2002. Akt/protein kinase B promotes organ growth in transgenic mice. Mol. Cell. Biol. 22, 2799–2809.

Skvorak, K.J., Paul, H.S., Dorko, K., Marongiu, F., Ellis, E., Chace, D., Ferguson, C., Gibson, K.M., Homanics, G.E., Strom, S.C., 2009. Hepatocyte transplantation improves phenotype and extends survival in a murine model of intermediate maple syrup urine disease. Mol. Ther.: J. Am. Soc. Gene Ther. 17, 1266–1273.

Soares, H.P., Ni, Y., Kisfalvi, K., Sinnett-Smith, J., Rozengurt, E., 2013. Different patterns of Akt and ERK feedback activation in response to rapamycin, active-site mTOR inhibitors and metformin in pancreatic cancer cells. PloS One 8, e57289.

Soriano, S., Llorens, J.V., Blanco-Sobero, L., Gutierrez, L., Calap-Quintana, P., Morales, M.P., Molto, M.D., Martinez-Sebastian, M.J., 2013. Deferiprone and idebenone rescue frataxin depletion phenotypes in a Drosophila model of Friedreich's ataxia. Gene 521, 274–281.

Stuwe, S.H., Goetze, O., Arning, L., Banasch, M., Schmidt, W.E., Schols, L., Saft, C., 2011. Hepatic mitochondrial dysfunction in Friedreich ataxia. BMC Neurol. 11, 145.

Sun, H., Olson, K.C., Gao, C., Prosdocimo, D.A., Zhou, M., Wang, Z., Jeyaraj, D., Youn, J.Y., Ren, S., Liu, Y., et al., 2016. Catabolic defect of branched-chain amino acids promotes heart failure. Circulation 133, 2038–2049.

Taneike, M., Nishida, K., Omiya, S., Zarrinpashneh, E., Misaka, T., Kitazume-Taneike, R., Austin, R., Takaoka, M., Yamaguchi, O., Gambello, M.J., et al., 2016. mTOR hyperactivation by ablation of tuberous sclerosis complex 2 in the mouse heart induces cardiac dysfunction with the increased number of small mitochondria mediated through the down-regulation of autophagy. PloS one 11, e0152628.

Tobias, D.K., Mora, S., Verma, S., Lawler, P.R., 2018. Altered branched chain amino acid metabolism: toward a unifying cardiometabolic hypothesis. Curr. Opin. Cardiol. 33, 558–564.

Tong, M., Zablocki, D., Sadoshima, J., 2020. The role of Drp1 in mitophagy and cell death in the heart. J. Mol. Cell Cardiol. 142, 138–145.

Tong, W.-H., 2017. Iron-sulfur proteins and human diseases. In: Rouault, T.A. (Ed.), Iron-sulfur Clusters in Chemistry and Biology. De Gruyter, Berlin, pp. 227–272.

Tong, W.H., Maio, N., Zhang, D.L., Palmieri, E.M., Ollivierre, H., Ghosh, M.C., McVicar, D.W., Rouault, T.A., 2018. TLR-activated repression of Fe-S cluster biogenesis drives a metabolic shift and alters histone and tubulin acetylation. Blood Adv. 2, 1146–1156.

Tong, W.H., Rouault, T.A., 2006. Functions of mitochondrial ISCU and cytosolic ISCU in mammalian iron-sulfur cluster biogenesis and iron homeostasis. Cell Metabol. 3, 199–210.

Vasquez-Trincado, C., Patel, M., Sivaramakrishnan, A., Bekeova, C., Anderson-Pullinger, L., Wang, N., Tang, H.Y., Seifert, E.L., 2021. Adaptation of the heart to Frataxin depletion: evidence that integrated stress response can predominate over mTORC1 activation. Hum. Mol. Genet.

Wang, H., Shi, H., Rejan, M., Canarie, E.R., Hong, S., Simoneschi, D., Pagano, M., Bush, M.F., Stoll, S., Leibold, E.A., Zheng, N., 2020. FBXL5 Regulates IRP2 Stability in Iron Homeostasis via an Oxygen-Responsive [2Fe2S] Cluster. Mol. Cell. 78, 31–41.

Wende, A.R., O'Neill, B.T., Bugger, H., Riehle, C., Tuinei, J., Buchanan, J., Tsushima, K., Wang, L., Caro, P., Guo, A., et al., 2015. Enhanced cardiac Akt/protein kinase B signaling contributes to pathological cardiac hypertrophy in part by impairing mitochondrial function via transcriptional repression of mitochondrion-targeted nuclear genes. Mol. Cell. Biol. 35, 831–846.

Zhang, S., Napierala, M., Napierala, J.S., 2019. Therapeutic prospects for Friedreich's ataxia. Trends Pharmacol. Sci. 40, 229–233.

Zhou, B., Tian, R., 2018. Mitochondrial dysfunction in pathophysiology of heart failure. J. Clin. Investig. 128, 3716–3726.